Available online at www.sciencedirect.com

SciVerse ScienceDirect

Acta Materialia 60 (2012) 2258–2264

Acta MATERIALIA

www.elsevier.com/locate/actamat

Dislocation starvation and exhaustion hardening in Mo alloy nanofibers

C. Chisholm [a,b], H. Bei [c], M.B. Lowry [a,b], J. Oh [d], S.A. Syed Asif [d], O.L. Warren [d], Z.W. Shan [d,e], E.P. George [c,f], A.M. Minor [a,b,*]

[a] Department of Materials Science and Engineering, University of California, Berkeley, CA 94720, USA
[b] National Center for Electron Microscopy, Lawrence Berkeley National Laboratory, 1 Cyclotron Road, MS 72, Berkeley, CA 94720, USA
[c] Materials Science and Technology Division, Oak Ridge National Laboratory, Oak Ridge, TN 37831, USA
[d] Hysitron Inc., 9625 West 76th Street, Minneapolis, MN 55344, USA
[e] Center for Advancing Materials Performance from the Nanoscale, State Key Laboratory for Mechanical Behavior of Materials, Xi'an Jiaotong University, Xi'an 710049, People's Republic of China
[f] Department of Materials Science and Engineering, University of Tennessee, Knoxville, TN 37996, USA

Received 12 October 2011; received in revised form 14 December 2011; accepted 15 December 2011
Available online 1 March 2012

Abstract

The evolution of defects in Mo alloy nanofibers with initial dislocation densities ranging from 0 to $\sim 1.6 \times 10^{14}$ m^{-2} were studied using an in situ "push-to-pull" device in conjunction with a nanoindenter in a transmission electron microscope. Digital image correlation was used to determine stress and strain in local areas of deformation. When they had no initial dislocations the Mo alloy nanofibers suffered sudden catastrophic elongation following elastic deformation to ultrahigh stresses. At the other extreme fibers with a high dislocation density underwent sustained homogeneous deformation after yielding at much lower stresses. Between these two extremes nanofibers with intermediate dislocation densities demonstrated a clear exhaustion hardening behavior, where the progressive exhaustion of dislocations and dislocation sources increases the stress required to drive plasticity. This is consistent with the idea that mechanical size effects ("smaller is stronger") are due to the fact that nanostructures usually have fewer defects that can operate at lower stresses. By monitoring the evolution of stress locally we find that exhaustion hardening causes the stress in the nanofibers to surpass the critical stress predicted for self-multiplication, supporting a plasticity mechanism that has been hypothesized to account for the rapid strain softening observed in nanoscale bcc materials at high stresses.
Published by Elsevier Ltd. on behalf of Acta Materialia Inc.

Keywords: In situ transmission electron microscopy; Tensile testing; Digital image correlation; Exhaustion hardening; Dislocation starvation

1. Introduction

There are many theoretical and experimental studies indicating that mechanical size effects are related to dislocation mechanisms and the consequence of increased surface to volume ratios at the nanoscale [1–4]. There remains the question of whether the dislocation processes inherent to bulk bcc crystals are also valid in small volumes [5,6]. Due to delocalization of the core structure of screw dislocations in bcc metals, flow stresses are typically controlled by the ability to move screw dislocations [7–9]. It has been shown that small face-centered cubic volumes exhibit source exhaustion and dislocation starvation during deformation [10–17]. However, it remains to be shown whether these processes also operate in bcc crystals. Exhaustion and starvation in bcc materials has been suggested [9], but has not yet been clearly observed. In situ transmission electron microscopy (TEM) tensile techniques are uniquely poised to offer significant insights in this discussion. Tensile testing has the important advantage of homogeneous uniaxial loading over the entire gage section. Historically, however, in situ TEM tensile testing was a qualitative technique due to the difficulty of simultaneously recording force data and achieving a sample geometry with a well-defined gage section. The

* Corresponding author at: 1 Cyclotron Road, MS 72, Berkeley, CA 94720, USA. Tel.: +1 510 495 2749.
E-mail address: aminor@berkeley.edu (A.M. Minor).

1359-6454/$36.00 Published by Elsevier Ltd. on behalf of Acta Materialia Inc.
doi:10.1016/j.actamat.2011.12.027

recent development of quantitative small-scale mechanical testing techniques, such as microcompression testing [18], has evolved to include tensile geometries [19,20] that take advantage of the flexibility of focused ion beam (FIB) machining, but suffer from the drawbacks of FIB preparation-related artifacts [21,22]. A different approach is to use a FIB-free sample with a predefined gage section, such as a nanowire [23]. By testing the sample in a transmission electron microscope the plastic deformation processes can be directly observed and correlated with concurrently obtained high resolution mechanical data. Here we combine techniques of quantitative in situ tensile testing and digital image correlation (DIC) [24] to achieve direct measurement of the true local stress and strain during tensile deformation of bcc nanofibers. By achieving local measurement of the stress and strain in the sample during a specific deformation event we can gain valuable insights into the mechanisms of small-scale plasticity in bcc metals.

2. Experiments and methods

2.1. Nanofiber preparation and characterization

Mo alloy (Mo–10Al–4Ni at.%) nanofibers were prepared by arc melting and directional solidification of a Ni–45.5Al–9Mo (at.%) eutectic composite. A detailed description of the nanofiber synthesis procedures has been reported previously [25]. For the in situ experiments we used single crystal fibers with approximately square cross-sections and sizes (edge lengths of the square) ranging from ~150 to 550 nm and fiber axes along the $\langle 001 \rangle$ direction. Fibers were exposed on the composite surface by selectively etching the Ni–Al matrix with an 18 vol.% HCl + 8 vol.% H_2O_2 + distilled/deionized (DI) water mixture. The etching time was chosen to reveal at least 20 μm lengths of Mo alloy fibers, which were then rinsed in DI water and sonicated in methanol to remove any residue from the etching process.

The dislocation density of the nanofibers can be changed by pre-straining the NiAl–Mo composite after directional solidification [26,27]. To measure the dislocation density of the nanofibers a square grid was overlaid on a projected TEM image of the fibers and the number of intersections of dislocation and grid were counted. The dislocation density was calculated based on Ham's method [28] as:

$$\rho_{\perp} = \frac{2NA_p}{V \cdot L} \tag{1}$$

where N is the total number of intersections, A_p is the projected area, V is the total volume of the portion of the fiber being analyzed, and L is the total length of grid lines used in the analysis. The as-grown fibers are mostly dislocation free. An imposed pre-strain of 15% results in a dislocation density of the order of $1.6 \times 10^{14}\ m^{-2}$. Intermediate pre-strains result in intermediate dislocation densities, but their distribution is not uniform along the fiber length. A detailed investigation of the dislocation density of the fibers as a function of pre-strain can be found elsewhere [26].

2.2. Experimental set-up

In situ TEM tensile testing of the Mo alloy nanofibers was conducted inside a JEOL 3010 microscope operated at 300 keV. A PI 95 TEM PicoIndenter system from Hysitron Inc. was used in displacement-controlled compression mode with a conductive diamond flat punch indenter to acquire raw load and displacement data at a displacement rate of 2 nm s^{-1}. The motion of the flat punch indenter was converted to tensile strain in the Mo alloy fibers via a MEMS fabricated "push to pull" (PTP) device [29]. The PTP device is microfabricated on a silicon on insulator wafer and has a semicircular end where the flat punch indenter contacts the device, as shown in Fig. 1. The PTP device has four identical springs distributed symmetrically at the corners so that a sample placed across the middle gap of the PTP device can be pulled in tension. The springs are designed to be stiffer in the lateral direction to ensure uniaxial tensile loading. By changing the dimensions of the springs the inherent stiffness of the PTP device can be tuned to optimize sample protection during handling, as well as the subsequent parameters of the test. The springs are arranged such that the force acting on them is parallel to the force on the tensile specimen. The device gap distance varies from 2 to 8 μm, allowing shorter or longer gage sections of a mounted sample.

The fibers were transferred to the PTP device using an Omniprobe micromanipulator in a FEI dual beam FIB/scanning electron microscope (SEM) (Fig. 1). Mo alloy fibers were attached with electron beam deposited platinum (Pt) to the micromanipulator, and their other ends cut with a focused 30 kV gallium (Ga) ion beam at a current of 10 pA to yield fibers ranging in length from 10 to 60 μm. The fibers were then transferred to the PTP device, where both ends were attached with electron beam deposited Pt. To avoid ion beam damage to the gage section during transfer of the nanofibers to the PTP device the fibers were only exposed to the ion beam locally, outside the gage sections used for the tensile tests.

2.3. Quantitative analysis of stress and strain

To calculate the engineering stress on the nanofiber its initial cross-sectional area and the force applied were determined. The initial cross-sectional area of the fibers is assumed to be square, as SEM images show this geometry is favored by the fibers. To measure the initial cross-sectional area the nanofibers were first tilted about their longitudinal axes in the TEM to a zone axis condition. For example, when tilted to the $\langle 110 \rangle$ zone axis the fiber edge is orthogonal to the electron beam and the projected width is considered to be equal to the fiber edge width. If tilted to ZA = $\langle 100 \rangle$ the projected width is equal to the diagonal of the cross-section. Ideally, four projected widths, at ZA = $\langle 110 \rangle$,

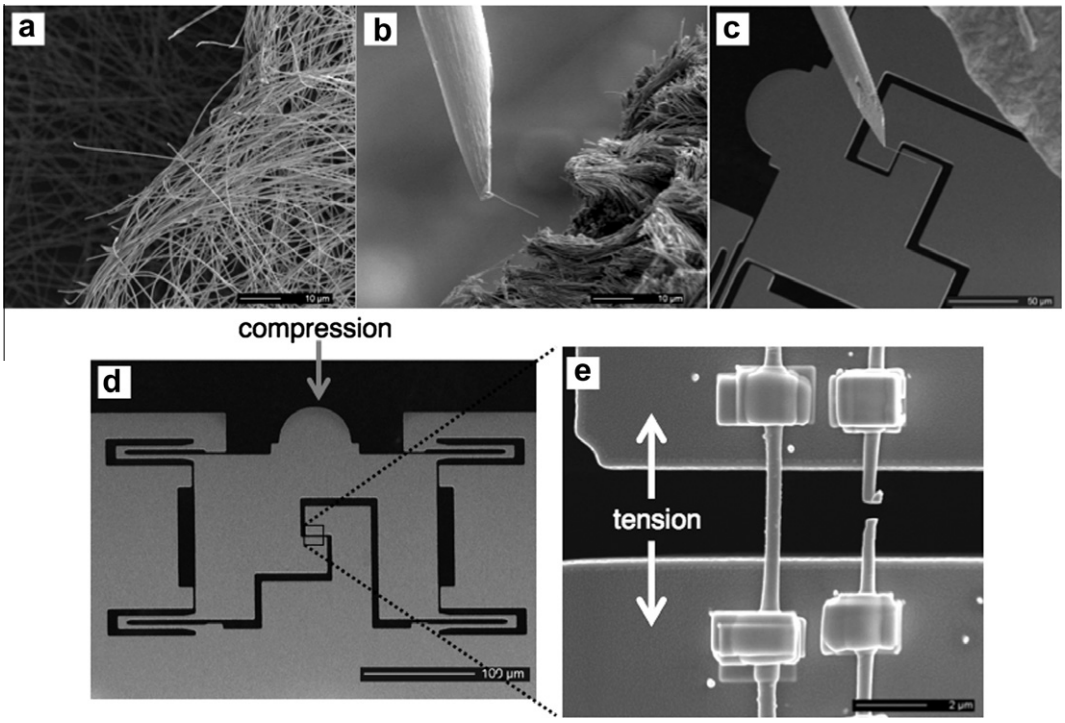

Fig. 1. (a) Mo alloy nanofibers, with tailorable dislocation densities, after etching of the NiAl matrix. (b) The fibers are picked up with a micromanipulator and (c) transported to the PTP device. The PTP device, micromanipulator and attached fiber, and in the upper right corner the Pt gas injection system, are shown. (d) SEM micrograph of the PTP device, with a higher magnification image (e) of the reusable gap across which different fibers can be mounted.

$\langle 100\rangle$, $\langle 210\rangle$, and $\langle 310\rangle$ were acquired to obtain an average edge width. The latter three require the geometric consideration of a perfectly square cross-section. The projected images were then used to measure the fiber cross-section along the $\langle 110\rangle$ width (referred to henceforth as the edge width) and the initial cross-sectional area calculated as the square of the measured edge dimension. It should be noted here that not all fibers have perfectly square cross-sections: some tend to be rectangular, and some have rounded corners. Therefore, the procedure outlined above leads to some uncertainty in the estimated cross-sectional areas and, in turn, the calculated stresses.

The raw force is taken to be the force applied to the combination of the sample and the PTP device, and the raw displacement is taken to be the motion of the flat punch indenter. The spring constant of the empty PTP device used for these experiments was measured after sample fracture and found to be 330 N m^{-1}. The force applied to the sample can be determined by subtracting the contribution of the PTP device from the raw force data. The engineering strain was calculated by dividing the raw displacement data by the initial gage length, measured by SEM as the length between the two attachment points. Here too it should be noted that the calculated strain may be overestimated because the raw displacement includes not only the contribution from the gage length but also those from other parts. For example, the potential deformation resulted from the locations where the fibers were attached to the PTP device with platinum and from the contact point between the flat punch indenter and the semicircular end of the PTP.

To better analyze any hardening that may have occurred during the tests the true stress and strain at a local area of necking was directly calculated from the in situ videos. DIC was applied to the still frames extracted from the recorded videos to measure the local instantaneous projected area and local elongation of the sample. The cross-sectional area is assumed to remain square during plastic deformation, as indicated by SEM micrographs of some of the deformed fibers after failure, and is used to calculate the local true stress. The local gage length was chosen individually for each fiber to be large enough to fully encompass the local area of interest. Surface features were typically used as markers for the DIC analysis to avoid any diffraction contrast effects as the fiber deformed. The location of the surface features was also factored into the determination of the gage length used for each DIC analysis.

3. Results

3.1. Nominally dislocation free

Most as-grown fibers can be considered nominally dislocation free, providing an interesting way to examine the deformation of a "perfect" material. For example, an as-grown fiber 160 nm in edge width was prepared using the methods described above to have a gage length of 5 μm, as shown in Fig. 2. Bright field diffraction contrast imaging

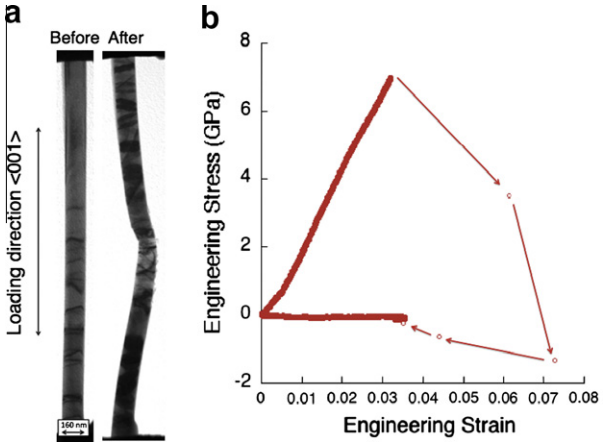

Fig. 2. Mechanical behavior of an as-grown nanofiber without dislocation. (a) Before and after TEM micrographs of the Mo alloy nanofiber with no dislocations prior to tensile testing. The lines of contrast in the before image are bend contours. (b) The engineering stress–strain curve shows that the sample is loaded elastically until 7 GPa, when the sample suddenly yields, exhibiting extreme strain softening and uncontrolled elongation past 7% engineering strain for a full load drop. After elongation the sample was compressed as the feedback loop of the displacement control caught up, resulting in buckling of the nanofiber.

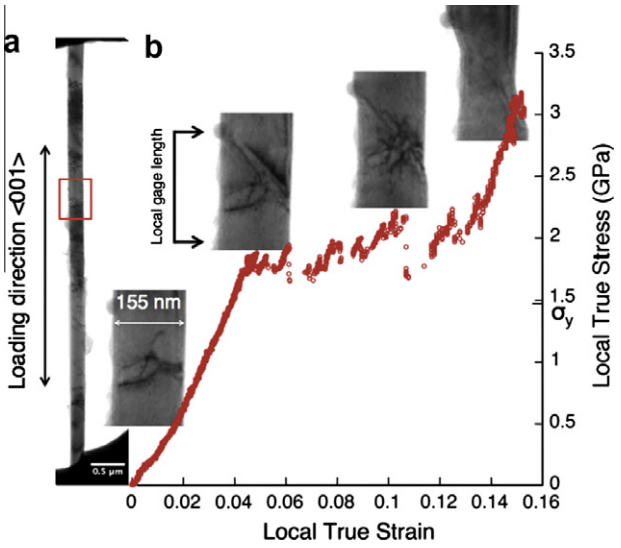

Fig. 3. Mechanical behavior of an as-grown nanofiber with pre-existing tangled dislocations (a) TEM micrograph of a Mo alloy nanofiber with an intermediate dislocation density. Packets of dislocations are present throughout the fiber and debris from the etching process can be seen along the sides. (b) Local true stress–strain curve generated using DIC, with a time series of the local area being analyzed shown along the curve. From left to right: the initial dislocation structure; at 1.56 GPa the spiral arm source begins to activate; the dislocation structure after the load drop; final necked region at 3 GPa after the spiral arm source was deactivated.

by TEM (Fig. 2a) showed that the sample prior to testing had a number of bend contours, but no dislocations. The sample is elastically loaded along its ⟨0 0 1⟩ axis until 3.3% engineering strain, when sudden catastrophic elongation occurs (see Supplementary material video 1), which is presumably the result of massive strain softening after yielding at the very high stress of ~7 GPa. The engineering stress–strain curve shown in Fig. 2b shows that by the time the sample fully unloads it has undergone 7.1% engineering strain before feedback control of the flat punch indenter can catch up with the burst and correct for it, resulting in compression back to 3.3% strain and buckling of the fiber. This uncontrolled elongation occurs in less than one video frame, or 0.033 of a second, and is consistent with previous compression results of as-grown fibers of the same alloy [27] and in situ TEM compression tests of FIB machined Mo pillars that were annealed to be dislocation free [22], both of which showed sudden plastic collapse after yielding. Unlike the micropillars in compression, however, the critical resolved shear stress for the $(-1\,1\,2)[-1\,1\,-1]$ slip system was determined to be 3.3 GPa or $G/34$ for our fiber, which is lower than the 4.6 GPa, or $G/25$, seen in compression [27]. Presumably this discrepancy is due to the longer gage section of our fiber compared with that of the micropillars, which increases the surface area available for heterogeneous dislocation nucleation. This notion is consistent with the results of recent in situ tensile tests of as-grown Mo alloy fibers by SEM [30]: if a sufficiently large number of long gage length specimens are tested a wide range of yield strengths is obtained, ranging from the very high theoretical strength measured in small gage length compression specimens [27] to as much as one order of magnitude lower strengths not seen in the Mo alloy micropillars.

3.2. Intermediate dislocation density

In some cases the as-grown nanofibers contained a number of dislocations even though they were not pre-strained. One example of this is shown in Fig. 3. An as-grown fiber, 155 nm in edge width, was prepared using the methods described above to have a gage length of 8 μm. Bright field TEM (Fig. 3a) of the nanofiber before testing shows that the sample contains groups of dislocations throughout. The sample was loaded along its ⟨0 0 1⟩ fiber axis and dislocation motion was first observed at a local true stress of 1.47 GPa, along the linear portion of the curve in Fig. 3 (see Supplementary material video 2). It should be noted that the yield strength for these intermediate fibers, as shown in their respective stress–strain curves, is taken to be when the first dislocation motion is observed. This initial dislocation motion does not necessarily coincide with a significant change in the slope of the stress vs. strain curve, which typically coincides with a shape change (necking). Fig. 3b shows the local true stress–strain curve for the necking region as calculated using DIC with images of the fiber at notable points overlaid on the curve. At a true stress of 1.56 GPa what appears to be a spiral arm dislocation source begins to operate, seen in Fig. 3b(ii), which leads to necking in the same area at 1.77 GPa. As deformation proceeds the number of dislocations in the necked region decreases (Fig. 3b(iii)–(iv)). As seen from the stress–strain curve, the decrease in dislocation density can be directly correlated with an increase in local stress. At a stress of 2.28 GPa the spiral arm source shuts down

(Fig. 3b(iv)) and the sample begins to elastically load again. This is due to a combination of both dislocation starvation (i.e. the initial dislocations have been annihilated) and dislocation source exhaustion (i.e. the spiral arm source has been deactivated).

As mentioned previously, it is possible to achieve intermediate starting dislocation densities by pre-straining the alloy before extracting the nanofibers. An example of this is shown in Fig. 4. Here a 9% pre-strained fiber with a 310 nm edge width contains exactly five dislocations along the 4.5 μm gage length. Crystallographic analysis ($g \cdot b$) of the dislocations prior to the test indicated that the dislocations had a Burger's vector of type $b = \frac{1}{2}\langle 1\,1\,1\rangle\{1\,1\,2\}$, but their character (edge or screw) could not be uniquely determined. Fig. 4 shows the results from a test that drove all five dislocations out of the sample after loading the fiber to an engineering strain of 1.1% (see Supplementary material video 3). By correlating the stress–strain data with the in situ TEM video it can be seen that the first dislocation (labeled dislocation 5 in Fig. 4) escapes from the fiber at 297 MPa, although the curve (Fig. 4a) shows no specific indication of this. The mechanical annealing of the four remaining dislocations subsequently occurs at progressively higher stresses. Each time, the dislocation escapes from the fiber with no apparent indication in the stress vs. strain curve. Fig. 4b shows images of the wire throughout the progression of mechanical annealing with the dislocation escape points marked on the curve in Fig. 4a.

Fig. 5 shows a second example of a 9% pre-strained fiber with an intermediate starting dislocation density. As can be seen in Fig. 5b, the fiber started with four dislocations near the bottom of the wire. Analysis of the dislocations prior to

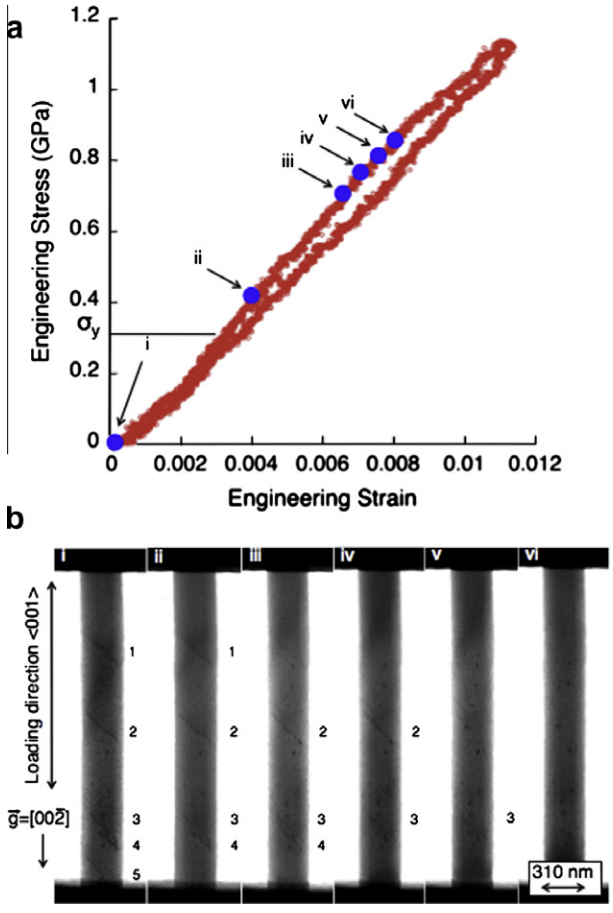

Fig. 4. Mechanical annealing of a nanofiber with 9% pre-strain. (a) Engineering stress–strain curve (loading and unloading) of an intermediate dislocation density fiber that displays both exhaustion hardening and dislocation starvation. (b) Time series of a fiber tilted to the [1 0 0] zone axis and loaded in the ⟨0 0 1⟩ direction, at the points indicated on the curve. (i) At 0 GPa there are five $b = \frac{1}{2}\langle 1\,1\,1\rangle\{1\,1\,2\}$ dislocations, (ii) at 0.4 GPa the first dislocation is annihilated, (iii) and the second follows at 0.68 GPa. (iv–vi) The remaining dislocations are annihilated at roughly 50 MPa increments. Unloading after the dislocations are eliminated results in essentially full strain recovery.

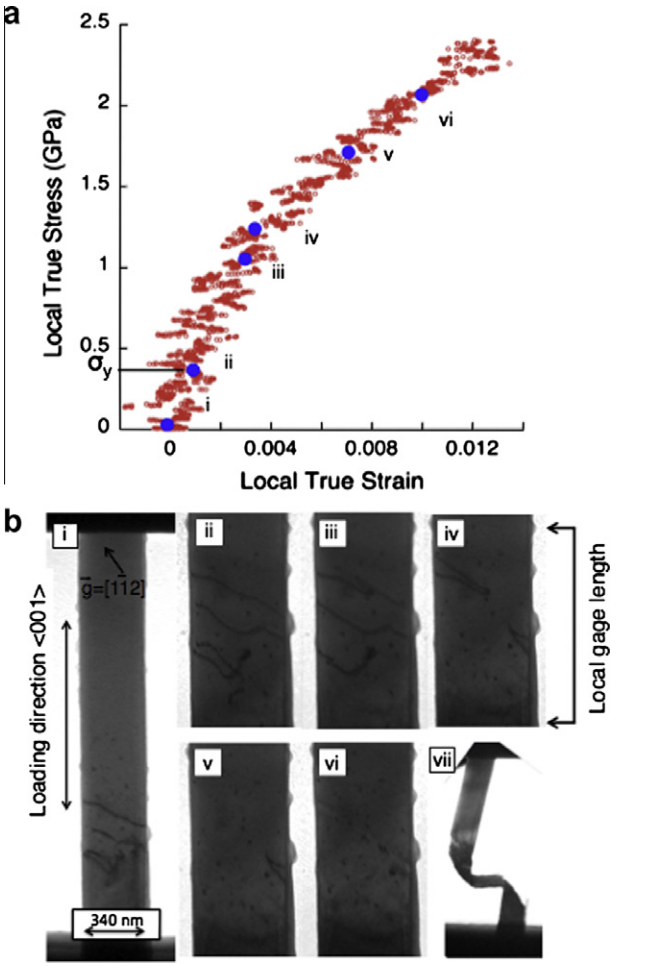

Fig. 5. Mechanical annealing and the subsequent catastrophic deformation of a nanofiber with 9% pre-strain. (a) True local stress–strain, calculated using DIC. The noise of the analysis is less than 0.3 of a pixel over the relatively small range of strain. (b) (i) Initial dislocation structure of the entire length of the wire. (ii–vi) Higher magnification images of the selected region analyzed by DIC. The region corresponds to the dislocations near the bottom of the full wire shown in (i). (ii) Dislocations start to move around the bulk yield value of 300 MPa. (iii)–(v) Dislocations are progressively annihilated as the stress increases. (vii) A low magnification image of the fiber after it catastrophically elongates and then buckles as feedback control compensates for the uncontrolled elongation by putting the fiber in compression.

the test again indicated that the dislocations all had a Burger's vector of type $b = \frac{1}{2}\langle 1\,1\,1\rangle\{1\,1\,2\}$, but their character (edge or screw) could not be uniquely determined. The nanofiber had an edge width of 340 nm and a 5.25 μm gage length. The nanofiber was strained until failure (see Supplementary material video 4) and DIC was used to analyze the true stress and strain around the local area of yielding, as shown in Fig. 5a. An additional advantage of using DIC to determine the strain is that any drift during the test (as can be noticed in Supplementary material video 4) is effectively removed from the mechanical data. The first dislocation begins to move at 317 MPa, followed by progressive mechanical annealing of the dislocations as they straighten and escape from the nanofiber as the stress increases. At 2.39 GPa catastrophic yielding involving rapid strain softening occurs (similar to the nanofiber with no initial dislocations) and the nanofiber is left thinned and heavily dislocated, as shown in Fig. 5b(vii).

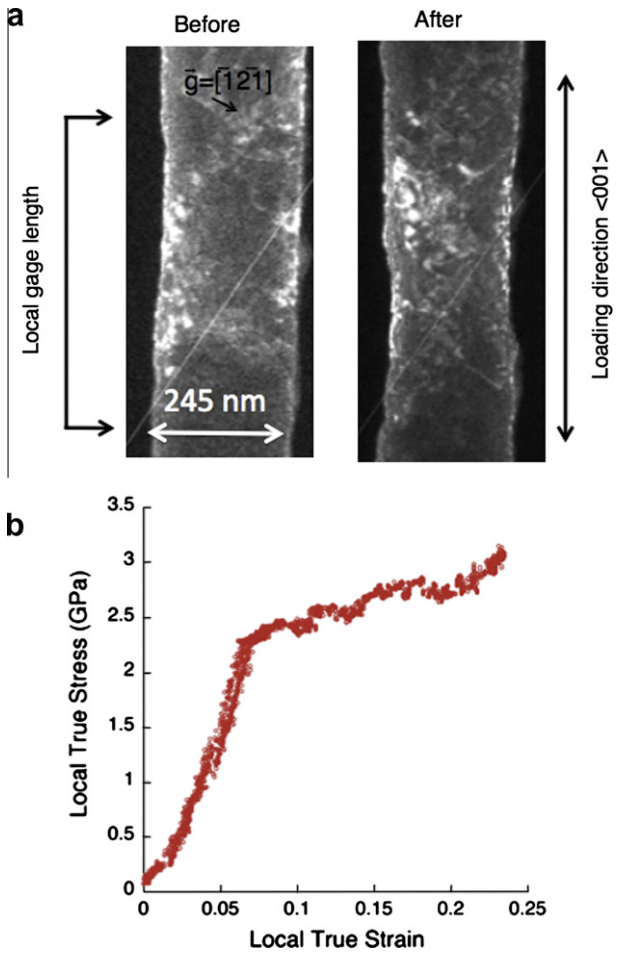

Fig. 6. Mechanical behavior of a nanofiber with 15% pre-strain. (a) TEM dark field micrographs of a heavily dislocated nanofiber before and after the tensile test. (b) Local true stress–strain curve, using DIC, for the portion of the nanofiber shown in (a). The sample is loaded linearly to a true stress of 2.2 GPa, when the nanofiber begins to neck. Plastic deformation and hardening is evenly sustained with a few minor load drops corresponding to slip events.

3.3. Heavily pre-strained

A 15% pre-strained nanofiber is shown in Fig. 6, for which a very high starting dislocation density of $\sim 1.61 \times 10^{14}\,\mathrm{m}^{-2}$ does not lead to as clear a picture of the hardening response as the nanofibers with intermediate dislocation densities (see Supplementary material video 5). The 15% pre-strained fiber has an edge width of 245 nm and was attached to the PTP device with a gage length of 8 μm. It was loaded in tension along the $\langle 0\,0\,1\rangle$ fiber axis and dislocation motion can be observed even in the linear region of the local true stress–strain curve (Fig. 6b). At a local true stress of 2.1 GPa the sample begins to neck. After necking begins there is sustained plastic deformation, accompanied by hardening and slip events leading to load drops. However, due to the large number of dislocations in the necked region it is unclear from this experiment which hardening processes are operating. Yield followed by sustained plasticity correspond well with what has been observed previously in compression tests of 15% pre-strained Mo alloy pillars [27].

4. Discussion

By loading the bcc Mo alloy fibers in tension, near uniform stresses with negligible stress concentrations can be achieved, giving a clear window into the role that dislocation density plays in deformation behavior in nanostructures. By observing the deformation in situ by TEM the evolution of both the dislocation density and stress in the material could be directly correlated.

Exhaustion hardening refers to the process by which a decrease in active dislocation density can lead to hardening in a material because it becomes progressively starved of dislocations that can flow at a given stress level. As this dislocation starvation increases and dislocation sources are exhausted, the flow stress of the sample increases, leading to hardening. Our results show that hardening due to both dislocation starvation and source exhaustion occurs in the Mo alloy nanofibers. After the sample has reached a dislocation starved or exhausted state, yielding is followed by catastrophic strain softening. Essentially, the progressive exhaustion of dislocations leads to a situation similar to that in samples with no initial dislocations, where elastic loading is followed by catastrophic strain softening upon yielding.

Recent computational simulations by Weinberger and Cai proposed a dislocation self-multiplication mechanism unique to bcc small volumes [2]. In their paper they found that, above a critical stress (σ_C), the combined effect of image forces and the core spreading in bcc screw dislocations can cause a single nucleation event to lead to an avalanche of dislocations and rapid strain softening. While the time resolution of our in situ tensile tests is much too low to directly confirm this mechanism, our observation of dislocation starvation/exhaustion followed by yielding and catastrophic strain softening is consistent with their proposed

mechanism. For example, Fig. 5 shows exhaustion hardening from 317 MPa to 2.39 GPa, at which point the nanofiber is starved of dislocations and sudden catastrophic yielding occurs. In comparison with the model by Weinberger and Cai, our experimental results are consistent with an idea that there is a critical stress for the self-multiplication mechanism, since catastrophic yielding was seen to occur either at high stresses in a dislocation-free nanofiber or in pre-strained wires after they had hardened to a higher flow stress due to the exhaustion of dislocations.

Interestingly, a common feature in most of our in situ tests of nanofibers with pre-existing dislocations was that the first observable dislocation motion occurred at values close to the bulk Mo yield strength of ~400 MPa. If we define "yield" as the first movement of dislocations, then our nanofibers that started with some dislocations actually yielded at the same value as bulk Mo. However, nanofibers have only a fraction of the defects that a bulk sample does for the same dislocation density. If these numbers are sufficiently small, the processes that generate sustained plasticity do not occur in nanoscale volumes at these lower stresses, due in part to escape of glissile defects to the surface (dislocation starvation).

5. Summary

The effect of initial dislocation density on the deformation processes of single crystal Mo alloy nanofibers was investigated by quantitative in situ TEM tensile testing. Nanofibers ranging from 140 to 370 nm edge width were used with dislocation densities ranging from 0 to 1.6×10^{14} m^{-2}. Nanofibers with no initial dislocations deformed elastically until a sudden catastrophic yield event. Nanofibers with a high initial dislocation density exhibited sustained plastic deformation after yielding at low stresses. The fibers with an intermediate initial dislocation density exhibited exhaustion hardening, in one case after the activation and subsequent deactivation of a spiral arm source and in the others after complete dislocation starvation. We found that after exhaustion hardening the nanofibers yielded catastrophically, consistent with the self-multiplication process hypothesized to account for rapid strain softening in nanoscale bcc materials at high stresses.

Acknowledgements

This work was supported by the Center for Defect Physics, an Energy Frontier Research Center funded by the US Department of Energy, Office of Science, Basic Energy Sciences. H.B. was supported by the US Department of Energy, Basic Energy Sciences, Materials Sciences and Engineering Division. PTP device development was funded by a DOE SBIR Phase II grant (DE-FG02-07ER84813) awarded to Hysitron Inc. The in situ TEM work was performed at the National Center for Electron Microscopy, Lawrence Berkeley National Laboratory, which is supported by the US Department of Energy under Contract No. DE-AC02-05CH11231. The authors thank M. Mills for thoughtful discussions and C. Eberl for sharing his expertise on using DIC analysis. Z.W.S. was also supported by the NSFC (50925104) and the 973 program of China (2010CB631003).

Appendix A. Supplementary material

Supplementary data associated with this article can be found, in the online version, at doi:10.1016/j.actamat.2011.12.027.

References

[1] Rao SI, Dimiduk DM, Parthasarathy TA, Uchic MD, Tang M, Woodward C. Acta Mater 2008;56:3245–59.
[2] Weinberger CR, Cai W. PNAS 2008;105:14304–7.
[3] Uchic MD, Shade PA, Dimiduk DM. Annu Rev Mater Sci 2009;39:361–86.
[4] Greer JR, De Hosson JTM. Prog Mater Sci 2011;56:654–724.
[5] Louchet F, Kubin LP, Vesely D. Philos Mag A 1979;39:433–54.
[6] Christian JW. Metall Trans A 1983;14:1237–56.
[7] Seeger A, Holzwarth U. Philos Mag 2006;86:3861–92.
[8] Šesták B, Seeger A. Phys Status Solidi B 1971;43:433–44.
[9] Schneider AS, Clark BG, Frick CP, Gruber PA, Arzt E. Philos Mag Lett 2010;90:841–9.
[10] Uchic MD, Shade PA, Dimiduk DM. JOM 2009;61:36–41.
[11] Shan ZW, Mishra RK, Syed Asif SA, Warren OL, Minor AM. Nature Mater 2008;7:115–9.
[12] Kiener D, Minor AM. Acta Mater 2011;59:1328–37.
[13] Oh SH, Legros M, Kiener D, Dehm G. Nature Mater 2009;8:95–100.
[14] Benzerga AA. J Mech Phys Solids 2009;57:1459–69.
[15] Lee S-W, Han SM, Nix WD. Acta Mater 2009;57:4404–15.
[16] Lee S-W, Nix WD. Mater Sci Eng A 2010;527:1903–10.
[17] Ng KS, Ngan AHW. Acta Mater 2009;57:4902–10.
[18] Uchic MD, Dimiduk DM, Florando JN, Nix WD. Science 2004;305:986–9.
[19] Kiener D, Grosinger W, Dehm G, Pippan R. Acta Mater 2008;56:580–92.
[20] Kiener D, Minor AM. Nano Lett 2011.
[21] Bei H, Shim S, Miller MK, Pharr GM, George EP. APL 2007;91:111915.
[22] Lowry MB, Kiener D, LeBlanc MM, Chisholm C, Florando JN, Morris JW, et al. Acta Mater 2010;58:5160–7.
[23] Zhu Y, Espinosa HD. PNAS 2005;102:14503–8.
[24] Eberl C, Gianola DS, Thompson R. MatLab Central. Natick (MA): The Mathworks Inc.; 2006 (File i.d. 12413).
[25] Bei H, George EP. Acta Mater 2005;53:69–77.
[26] Phani PS, Johanns KE, Duscher G, Gali A, George EP, Pharr GM. Acta Mater 2011;59:2172–9.
[27] Bei H, Shim S, Pharr GM, George EP. Acta Mater 2008;56:4762–70.
[28] Ham RK. Philos Mag 1961;6:1183–4.
[29] Guo H, Chen K, Oh Y, Wang K, Dejoie C, Syed Asif SA, et al. Nano Lett 2011:0–6.
[30] Johanns K, Sedlmayr A, Sudarshan Phani P, Monig R, Kraft O, George EP, et al. J Mater Res 2011, in press, doi:10.1557/jmr.2011.298.